# LB-SciFi: Online Learning-Based Channel Feedback for MU-MIMO in Wireless LANs

Pedram Kheirkhah Sangdeh\*, Hossein Pirayesh\*, Aryan Mobiny<sup>†</sup>, and Huacheng Zeng\*

\*CSE Dept, Michigan State University 

†ECE Dept, University of Houston

Email: {sangdeh, pirayesh, hzeng}@msu.edu, amobiny@uh.edu

Abstract-Multi-user MIMO (MU-MIMO) is a key technology for current and next-generation wireless local area networks (WLANs). While it has widely been deployed in WLANs, its potential is not fully exploited in real-world systems. This can be attributed to the large airtime overhead induced by channel acquisition in existing MU-MIMO protocols, which significantly compromises the throughput gain of MU-MIMO. In this paper, we present LB-SciFi, a learning-based channel feedback framework for MU-MIMO in WLANs. LB-SciFi takes advantage of recent advances in deep neural network autoencoder (DNN-AE) to compress channel state information (CSI) in 802.11 protocols, thereby conserving airtime and improving spectral efficiency. The key component of LB-SciFi is an online DNN-AE training scheme, which allows an AP to train DNN-AEs by leveraging the side information of existing 802.11 protocols. With this training scheme, DNN-AEs are capable of significantly lowering the airtime overhead for MU-MIMO while preserving its backward compatibility with incumbent Wi-Fi client devices. We have implemented LB-SciFi on a wireless testbed and evaluated its performance in indoor wireless environments. Experimental results show that LB-SciFi offers an average of 73% airtime overhead reduction and increases network throughput by 69% on average when compared to 802.11 feedback protocols.

Index Terms—MU-MIMO, Wi-Fi, beamforming, deep learning, explicit channel feedback

#### I. INTRODUCTION

The proliferation of wireless devices, combined with the growth of Internet-based wireless applications, has led to increasing demands for wireless services in indoor environments. As one of the largest wireless networks in real world, wireless local area networks (WLANs) carry the most wireless data traffic (even more than cellular networks) and play a pivotal role in our society. To meet the increasing demands for data services in WLANs, multi-user multiple-input multiple-output (MU-MIMO) is a key technology. It allows an access point (AP) to serve multiple users simultaneously and therefore can significantly improve the spectral efficiency. Given its potential, MU-MIMO has been specified in IEEE 802.11 standards [1], [2] and widely been deployed on commercial Wi-Fi devices, e.g., Wi-Fi routers, laptops, and phones.

In real-world WLANs, the downlink typically has higher demands for data services compared to the uplink. To support downlink MU-MIMO communications in WLANs, an AP needs to access short-term channel state information (CSI) for the construction of beamforming filters. The filters will then be used to project the precoded signals onto the AP's multiple antennas so that each user can decode its data packets. Thus,

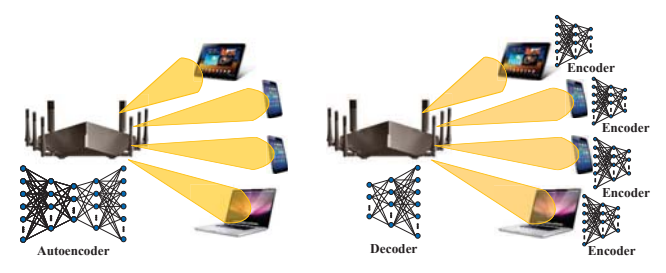
CSI at the AP is essential to enabling downlink MU-MIMO transmissions. There are two channel acquisition methods for an AP to obtain CSI: i) *implicit channel acquisition*, and ii) *explicit channel acquisition*. The implicit method is based on channel reciprocity. The AP infers the downlink CSI through the estimation of uplink CSI and periodic channel calibrations [3]. This method, however, requires an extra radio frequency (RF) chain on hardware or a sophisticated algorithm for channel calibration and may not be suited for implementation on low-cost Wi-Fi devices [4]–[6].

The explicit method is based on channel feedback over uplink over-the-air channel. Each user first estimates the downlink CSI and then reports the estimated CSI to the AP. Given its amenability to implementation, this method has been adopted by the IEEE 802.11 standards [1], [2] and been implemented on commercial Wi-Fi systems. However, due to its reliance on over-the-air CSI feedback, it suffers from large airtime overhead. This large overhead can be attributed to the large number of subcarriers in WLANs' OFDM modulation, each of which has a channel matrix to be reported. Existing 802.11 protocols may group subcarriers for CSI feedback to reduce the overhead. Such a naive scheme leads to an inferior beamforming performance and compromises the throughput gain of MU-MIMO. While there are many results of MU-MIMO in the literature, the CSI compression for 802.11 MU-MIMO protocols is highly overlooked.

In this paper, we study explicit channel acquisition in 802.11 MU-MIMO protocols with the objective of minimizing CSI feedback airtime overhead while preserving CSI feedback accuracy. Toward this objective, we propose a learning-based channel feedback framework (called LB-SciFi<sup>1</sup>) for 802.11 protocols to reduce their airtime overhead by taking advantage of deep neural network autoencoder (DNN-AE). Fig. 1 shows the basic idea of LB-SciFi, which is composed of two phases: online training and real-time exploitation. In the training phase, LB-SciFi trains DNN-AEs at the AP by leveraging side information from existing 802.11 protocols, and thus require no extra effort from user devices. In the *exploitation* phase, LB-SciFi uses the trained DNN-AEs to compress CSI for feedback. Given the redundancy of CSI and the effectiveness of DNN-AEs, LB-SciFi can reduce the airtime overhead significantly without sacrificing CSI feedback accuracy.

The main challenge in the design of LB-SciFi is the online

 $^{1}$ LB-SciFi stands for <u>L</u>earning-<u>B</u>ased compression for  $\Psi$  (<u>Sci</u>) and  $\Phi$  (<u>Fi</u>), which are the CSI for feedback in 802.11 MU-MIMO protocols [1], [2].



- (a) Online training.
- (b) Real-time exploitation.

Fig. 1: An overview of DNN-AEs for channel feedback compression in 802.11 MU-MIMO protocols.

training of DNN-AEs, which should be capable of capturing the kernel space of all possible channels in a given wireless environment through the learning of collected CSI at the AP. To address this challenge, we design an efficient training scheme for the DNN-AEs to collect, clear, and process the training data by leveraging side information in existing 802.11 MU-MIMO protocols. The proposed training scheme meticulously chooses the  $\psi$  and  $\phi$  angles from Givens Rotation (GR) as the DNN-AEs input based on power spectral entropy (PSE). Moreover, several important engineering problems have been addressed to make DNN-AEs work in real-world wireless environments.

The contributions of this paper are summarized as follows.

- We propose to employ DNN-AEs for CSI compression in 802.11 MU-MIMO protocols and design an online training scheme for DNN-AEs while imposing no computational burden on user devices.
- Based on the DNN-AEs, we design a learning-based channel feedback framework (LB-SciFi) for downlink MU-MIMO. This framework can dramatically reduce the CSI feedback airtime overhead for 802.11 MU-MIMO protocols without sacrificing CSI feedback accuracy.
- We build a prototype of LB-SciFi and evaluate its performance in real-world indoor environments. Our experimental results show that LB-SciFi reduces the CSI feedback airtime overhead by 73% and improves the throughput of MU-MIMO by 69% on average.

#### II. RELATED WORK

We focus our literature review on research efforts studying low-overhead channel acquisition methods for MU-MIMO transmissions in WLANs and cellular networks.

Channel Acquisition in WLANs: As the core technology of existing WLANs, MU-MIMO markedly improves users experience with high throughout and low latency. However, airtime overhead from channel acquisition is a real barrier toward fully exploiting the potential of MU-MIMO. Given the severity of this issue, research efforts have been devoted to studying the effect of channel acquisition parameters on network throughput or completely altering the channel acquisition paradigm to enhance network throughput [7]–[18].

Pioneering work [7]–[10] studied the underlying relationship between network throughput and channel acquisition parameters. The outcome was not surprising; full exploitation of MU-MIMO requires a timely CSI through a frequent channel

acquisition. The large airtime overhead, however, drastically compromises the throughput gain of MU-MIMO. [11]–[15] aimed at lowering the frequency of channel acquisitions to reduce channel feedback overhead for MU-MIMO protocols. However, the airtime overhead was still too large. [16]–[18] revisited existing channel acquisition paradigm and explored new methods for efficient channel acquisition.

Thus far, there is no efficient method for CSI compression to reduce feedback overhead. Our work fills this gap by leveraging recent advances in artificial neural networks to compress CSI. The resultant CSI feedback will entail much less overhead compared to existing 802.11 protocols.

Channel Acquisition in Cellular Networks: Compared to WLANs, the need for low-overhead channel acquisition in cellular networks is appreciated earlier as the emergence of massive-MIMO revealed the drawbacks of traditional methods. To this end, the underlying correlation of CSI reports has been used for compression by removing the redundant information [19]–[24]. In particular, temporal correlation [19]–[21], spectral correlation [22]–[24], and spatial correlation [19], [25] have been explored to minimize the representation of CSI. Channel reciprocity [26]–[28] and outdated CSI [29] have also been studied to enhance the efficiency of channel acquisition.

Our work is orthogonal to these research efforts in the following two aspects: i) Our work focuses on indoor WLANs, which differ from cellular networks in terms of CSI format, network architecture, data collection, data processing, and system implementation. ii) While the above efforts focused on theoretical exploration, our work focuses on practical design based on real-world 802.11 protocols.

# III. PROBLEM DESCRIPTION

In this section, we first offer a primer of existing 802.11 MU-MIMO protocols and underscore their airtime overhead issue. Then, we state our design objectives and challenges.

#### A. Existing 802.11 MU-MIMO Protocols

Consider a WLAN as shown in Fig. 1(a), where a multi-antenna AP is serving a set of user devices (a.k.a. stations or STAs for brevity). The AP is equipped with  $N_{\rm ap}$  antennas, and an STA is equipped with  $N_{\rm sta}$  antennas. Due to the physical size and power limits, an STA typically has less antennas than an AP, i.e.,  $N_{\rm sta} < N_{\rm ap}$ . In such a WLAN, MU-MIMO is widely used to exploit the spatial degrees of freedom (DoF) of asymmetric antenna configuration by enabling the AP to serve multiple STAs simultaneously. To enable MU-MIMO in WLANs, protocols with explicit channel acquisition have been specified in the IEEE 802.11 standards [1], [2]. Fig. 2 shows an existing 802.11 MU-MIMO protocol, which is composed of the following four phases:

 MU-MIMO Announcement: The AP selects a subset of STAs for the downlink MU-MIMO transmission based on some pre-defined criteria. After user selection, the AP broadcasts a Null Data Packet Announcement (NDPA) to inform the STAs of MU-MIMO transmission, followed by an NDP for those STAs to estimate downlink CSI.

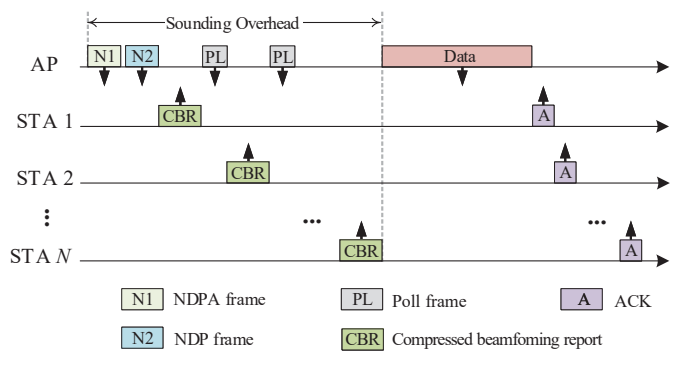


Fig. 2: An MU-MIMO protocol in IEEE 802.11ac [1].

- Channel Feedback: After estimating CSI, the selected STAs feed back their CSI to the AP sequentially following the poll frames from the AP.
- *Data Transmission:* Upon obtaining CSI from all the STAs, the AP uses CSI to construct beamforming filters and performs downlink data transmission.
- Acknowledgment: After decoding the data packets, all the STAs send an ACK/NACK to the AP to indicate the success/failure of their packet detection.

In the channel feedback phase, if an STA sends raw CSI to the AP, it entails a huge amount of airtime overhead and thus negates the throughput gain of MU-MIMO. To reduce the airtime overhead, 802.11 protocols have employed anglebased CSI feedback instead of raw CSI feedback in the spatial domain and specified subcarrier grouping in the spectral domain. We detail them below.

Angle Feedback in Spatial Domain: Referring to the protocol in Fig. 2, once an STA has received the NDP from the AP, it estimates the downlink CSI, i.e.,  $\mathbf{H}(k) \in \mathbb{C}^{N_{\mathrm{sta}} \times N_{\mathrm{ap}}}$ ,  $1 \leq k \leq N_{\mathrm{sc}}$ , where  $N_{\mathrm{sc}}$  is the number of valid subcarriers. Instead of reporting the complex entries of  $\mathbf{H}(k)$ , the STA reports two sets of angles ( $\mathbf{\Psi}$  and  $\mathbf{\Phi}$ ) to the AP to reduce the feedback overhead. A high-level description of computing  $\mathbf{\Psi}$  and  $\mathbf{\Phi}$  is given in Alg. 1. This conversion is also known as Givens rotations. Details of computing the angles can be found in [30]. With these two sets of angles, the AP can reconstruct the essential spatial information of  $\mathbf{H}(k)$ , which suffices for beamforming operations at the AP.

In this method, the number of generated angles in  $\Psi$  is  $N_{\psi} = (N_{\rm ap}N_{\rm sta} - N_{\rm sta}^2/2 - N_{\rm sta}/2)N_{\rm sc}$ , so is the number of angles in  $\Phi$ . These angles need to be reported to the AP via the uplink over-the-air channels. In 802.11 standards [1], two types of quantization are specified for CSI feedback:

- Type 0: 5 bits for angles in  $\Psi$  and 7 bits for angles in  $\Phi$ ,
- Type 1: 7 bits for angles in  $\Psi$  and 9 bits for angles in  $\Phi$ .

Subcarrier Grouping in Spectral Domain: In a typical environment of WLANs, adjacent subcarriers experience highly correlated channel responses from the medium. Therefore, instead of reporting CSI for every individual subcarrier, an STA may group multiple neighboring subcarriers together for CSI feedback. Per IEEE 802.11ac [1], the number of subcarriers in a group, denoted by  $N_{\rm g}$ , can be 1, 2, or 4.

Algorithm 1 A high-level description of computing  $\Psi$  and  $\overline{\Phi}$  at an STA specified in the IEEE 802.11ac/ax [1], [2].

```
Inputs: Estimated channel at an STA, i.e., \mathbf{H}(k)
     \mathbb{C}^{N_{\text{sta}} \times N_{\text{ap}}}, 1 \leq k \leq N_{\text{sc}}
 Outputs: Computed angles, i.e., \Psi and \Phi
 1: Set \Psi = \{\} and \Phi = \{\}
 2: for (k = 1; k \le N_{sc}; k++) do
           [\mathbf{U}, \ \mathbf{\Sigma}, \ \mathbf{V}] = svd(\mathbf{H}(k))
 3:
 4:
           \mathbf{V}' = \mathbf{V} (:, 1:N_{\mathrm{sta}})
          for (l = 1; l \le N_{\rm sta}; l++) do
 5:
                 \psi_k := phase\_extraction(\mathbf{V}'(:,l))
 6:
                 \phi_k := givens\_rotations(\mathbf{V}'(:,l))
 7:
                 \mathbf{\Psi} := \left\{ \mathbf{\Psi} \ \psi_k \right\} \text{ and } \mathbf{\Phi} := \left\{ \mathbf{\Phi} \ \phi_k \right\}
 8:
 9:
          end for
10: end for
11: Quantizing every angle in \Psi using p bits, p \in \{5,7\}
12: Quantizing every angle in \Phi using q bits, q = p + 2.
```

Large Airtime Overhead: Even with the spatial- and spectral-domain compression, 802.11 MU-MIMO protocols still come with a large airtime overhead, which significantly compromises the throughput of MU-MIMO [18], [31]. For example, for an STA with 4 antennas and an AP with 8 antennas, the CSI feedback could be as large as 19.7 kbit for 20 MHz bandwidth and 170.4 kbit for 160 MHz bandwidth. The problem of CSI feedback airtime overhead becomes increasingly acute as the evolution of WLANs is accommodating more subcarriers in a certain frequency band.

#### B. Our Objective

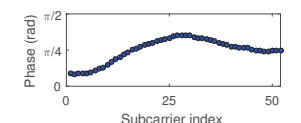
We aim to reduce the CSI feedback airtime overhead by taking advantage of recent advances in DNN-AEs, which have been successfully used for data compression and feature extraction in other fields. Toward this aim, we will compress the angles in  $\Psi$  and  $\Phi$  in the spectral domain by removing their information redundancy caused by channel correlation.

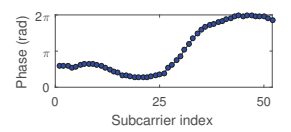
# IV. LB-SCIFI: A LEARNING-BASED FEEDBACK FRAMEWORK

To reduce the CSI feedback airtime overhead, we propose LB-SciFi for CSI compression. The core components of LB-SciFi are two DNN-AEs, which compress CSI at each STA and decompress CSI at the AP. Fig. 1 shows the basic idea of LB-SciFi, which is composed of two phases: *online training* and *real-time exploitation*. As shown in Fig. 1(a), the online training is done at the AP by taking advantage of the side information ( $\Psi$  and  $\Phi$ ) from existing 802.11 protocols. Once the training of DNN-AEs is completed, the AP broadcasts the DNN-AEs to all STAs and enters into the exploitation phase as shown in Fig. 1(b). In the exploitation phase, each STA uses DNN-AEs to compress its CSI and reports the compressed CSI to the AP. The AP uses DNN-AEs to decompress the received CSI for the construction of beamforming filters.

# A. DNN-AEs

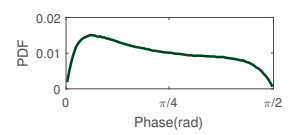
Autoencoder is a type of artificial neural network used to learn efficient data coding in a self-supervised manner. One

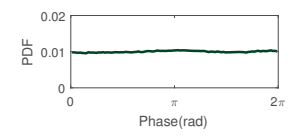




(a) An angle in  $\Psi$  on 52 subcarriers (measured PSE is 0.11). riers (measured PSE is 0.25).

Fig. 3: Angle instances in  $\Psi$  and  $\Phi$  as well as their PSE.





- (a) PDF of the angles in  $\Psi$ .
- (b) PDF of the angles in  $\Phi$ .

Fig. 4: Distribution of the measured angles over all subcarriers and at many locations in a real-world office environment.

of its applications is to learn a representation for a set of data for dimensionality reduction. Autoencoders are effectively used for solving many applied problems, ranging from face recognition to acquiring the semantic meaning of words. In this work, we take advantage of recent advances in DNN-AEs to compress CSI for 802.11 MU-MIMO protocols. We consider a DNN-AE as shown in Fig. 1, which is composed of two parts: encoder and decoder. The encoder will be used on each STA to compress its estimated CSI for feedback, and the decoder will be used to recover CSI at the AP.

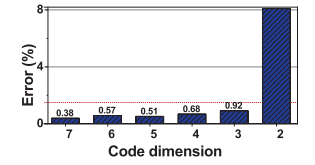
Compressibility of  $\Psi$  and  $\Phi$ : Before delving into the details of DNN-AEs, we introduce a metric to quantify compressibility of angles on an observation basis. The compressibility metric will lay the foundation for our design of DNN-AEs. Consider an angle sequence  $\overrightarrow{\theta} = [\theta_1, \theta_2, \cdots, \theta_K]$ . Denote its FFT output as  $\overrightarrow{\vartheta} = [\vartheta_1, \vartheta_2, \cdots, \vartheta_K]$ . Then, we define PSE of  $\overrightarrow{\theta}$  as follows:

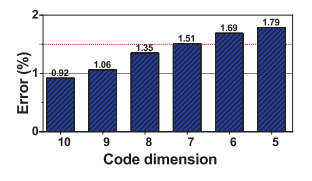
$$PSE(\overrightarrow{\theta}) = -\frac{1}{\log_2 K} \sum_{k=1}^K p(\vartheta_k) \log_2 p(\vartheta_k), \tag{1}$$

where  $p(\vartheta_k) = \frac{|\vartheta_k|^2}{\sum_{i=1}^K |\vartheta_i|^2}$  [32]. Apparently, the PSE of an angle sequence is bounded in [0 1]. PSE reflects the uncertainty or fluctuations of a measured angle over subcarriers. Intuitively, a low value of PSE indicates high compressibility, while a high value of PSE indicates low compressibility.

In WLANs, STAs are semi-stationary and work on a limited bandwidth. In such an environment, the channels between an AP and STAs are prone to be frequency-flat, and the channel responses on adjacent subcarriers are highly correlated. Fig. 3 exhibits an angle in  $\Psi$  and an angle in  $\Phi$  over 52 valid subcarriers in 20 MHz bandwidth at 2.484 GHz as well as their PSE values. It is evident that both PSE values are much less than 1, indicating the compressibility of the angles.

**Separate DNN-AEs for \Psi and \Phi:** For an STA, it needs to first compress  $\Psi$  and  $\Phi$ , and then report compressed  $\Psi$  and  $\Phi$  to the AP. A natural question to ask is whether an STA should use the same DNN-AE for both  $\Psi$  and  $\Phi$ . To answer this question, we empirically study the compressibility of the angles in  $\Psi$  and  $\Phi$ . Specifically, we collected the CSI





- (a) Error for  $\psi$  angles.
- (b) Error for  $\phi$  angles.

Fig. 5: Compression error for different code dimensions.

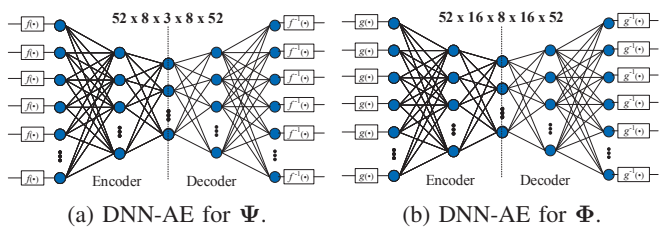


Fig. 6: Illustration of two different DNN-AEs for  $\Psi$  and  $\Phi$ .

angles for  $\Psi$  and  $\Phi$  at the STAs that were widely distributed in a real-world office environment, and plotted the probability density function (PDF) of the collected angles. Fig. 4 shows our measured results. We can see that the angles in  $\Psi$  is non-uniformly distributed, while the angles in  $\Phi$  are almost uniformly distributed. Based on collected CSI angles, the measured PSE of  $\Psi$  is 0.09, and the measured PSE of  $\Phi$ is 0.23. The measurement results indicate that the angles in  $\Psi$  and  $\Phi$  have different levels of compressibility. Given that the compression ratio is determined by a DNN-AE's structure (the ratio of dimension of the input layer to that of the latent layer), we employ two DNN-AEs for compressing  $\Psi$  and  $\Phi$ . **DNN-AEs Settings:** Another question to ask is about the parameter selection of the two DNN-AEs, including the number of layers, the number of neurons on each layer, quantization bits, and dimension of the latent layer. Unfortunately, there is no systematic approach that we can utilize to determine the optimal values for these parameters. Therefore, we focus only on the dimension of the latent layer (a.k.a. code dimension) as it is the most important parameter for a DNN-AE. Fig. 5 presents the compression error of DNN-AEs for different code dimensions. Using 1.5% error as reference, we select the code dimension that offers the best compression rate. As such, our design choices are  $52 \times 8 \times 3 \times 8 \times 52$  for  $\Psi$ 's DNN-AE and  $52 \times 16 \times 8 \times 16 \times 52$  for  $\Phi$ 's DNN-AE, as shown in Fig. 6.

# B. Online Training: Data Collection

As illustrated in Fig. 1, the AP takes advantage of existing 802.11 protocols to train the DNN-AEs. That is, AP and STAs perform downlink MU-MIMO transmissions using the 802.11 protocol as shown in Fig. 2. In the meantime, the AP trains the DNN-AEs using reported CSI (uncompressed  $\Psi$  and  $\Phi$ ) from the STAs. By doing so, the AP can train the DNN-AEs by collecting side information from the existing MU-MIMO protocol, and the training remains transparent to the STAs. In the course of data collection, care should be taken for the following two tasks.

**Avoiding Garbage-In/Garbage-Out:** To collect a meaningful dataset for training DNN-AEs, the AP needs to block out garbage CSI reports from STAs. In real WLANs, an STA

may fail in estimating accurate CSI due to various sources of errors such as time and frequency synchronization errors. As a garbage report has intrinsically a noise-like behavior, several dominant components exist in its spectral representation. Therefore, the PSE of such a report is high likely to be overly high. The AP leverages PSE metric in (1) and blocks out the sequences with abnormal PSE. The abnormality is detected by adjusting appropriate thresholds. In our experiment, we assumed that an abnormal angle in  $\Phi$  has PSE  $\geq 0.25$  and that an abnormal angle in  $\Phi$  has PSE  $\geq 0.5$ .

Avoiding Overrepresentation: Another important task of the AP is to prepare a balanced data set. In a typical WLAN, a *static* STA like smart TV remains at a fixed location without quitting the WLAN, while a *mobile* STA wanders through coverage range and may quit the WLAN for a while. A static STA may temporally experience correlated large-scale fading, making its historical CSI reports highly correlated. In light of this, the CSI reports from static STAs might be over-represented, making the DNN-AEs biased in favor of themselves. To avoid overrepresentation, the AP divides the PSE range into 100 uniform bins. If the AP receives 20 consecutive CSI samples of the same PSE value from the same STA, it will ignore the subsequent CSI samples from this STA, until the PSE value of its CSI samples changes. Here, PSE values within a PSE bin are considered the same.

#### C. Online Training: Data Preprocessing

After clearing and balancing the collected datasets, the AP preprocesses the datasets before feeding them into DNN-AEs for training. In what follows, we first describe the purpose of data preprocessing and then present the preprocessing procedure for the two sets of angles.

**Purpose of Data Preprocessing:** To avoid biased training and boost the convergence for DNN-AEs, we wish to obtain the training datasets with a normalized zero-mean PDF and uniform subcarrier-wise variance in the feasible space [33]. Such datasets are more likely to render an unbiased training for the DNN-AEs and yield a high compression ratio. Unfortunately, the collected angles in  $\Psi$  and  $\Phi$  do not meet these two conditions (normalized zero-mean distribution and flat subcarrier-wise variance). Therefore, we preprocess the collected datasets with the aim of rectifying their distributions to accelerate the training.

**Preprocessing of Angles in \Psi:** Fig. 7(a) shows the PDF and variance of the angles in  $\Psi$  before the preprocessing. As it can be seen, the angles in  $\Psi$  are non-uniformly distributed within their range. To alleviate this issue, we apply a rectification function  $f(\cdot)$  at the encoder and de-rectification function  $f^{-1}(\cdot)$  at the decoder, as shown in Fig. 6(a). Here, we employ  $f(\psi_k) = \alpha \left(\psi_k - \bar{\psi}\right)$  as the rectification function, where  $\bar{\psi}$  is the average of the angles in  $\Psi$  and  $\alpha$  is a normalization constant. In our experiments, we use  $\bar{\psi} = 0.68$  rad and  $\alpha = 1.12$ . After the rectification, the angles will have zero mean and uniform variance over different subcarriers, thereby improving the convergence of the DNN-AEs [34] and avoiding zigzag behavior in gradient descent algorithms [35].

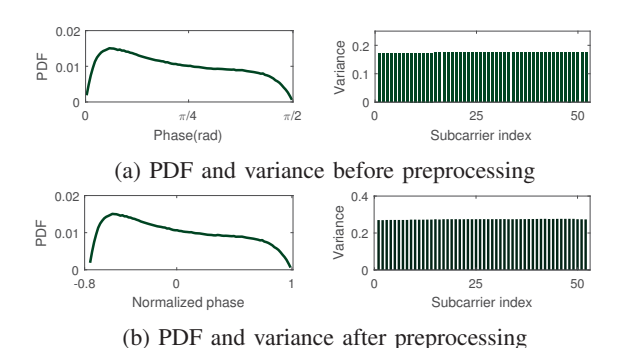
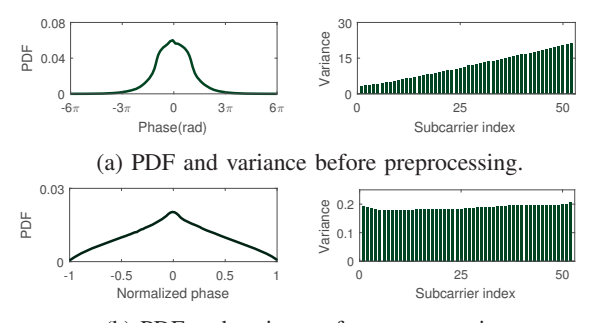


Fig. 7: The PDF and variance of the angles in  $\Psi$  before and after rectification.



(b) PDF and variance after preprocessing.

Fig. 8: The PDF and variance of the angles in  $\Phi$  before and after rectification.

Fig. 7(b) shows the PDF and variance of the angles in  $\Psi$  after the preprocessing. As it can be seen, the PDF is normalized and zero-mean after the preprocessing, which leads to a disciplined training for the corresponding DNN-AE.

**Preprocessing of Angles in \Phi:** Compared to  $\Psi$ , the preprocessing of  $\Phi$  is a bit more tricky. Fig. 8 shows the probability density function and subcarrier-wise variance of the angles in  $\Phi$  measured in real WLANs. The non-uniform probability distribution, non-uniform variance, high variance on each subcarrier, and the large range (even beyond  $[-4\pi, 4\pi]$ ) make the angles in  $\Phi$  unsuited for training. Preprocessing is needed to rectify the dataset to improve the convergence of the DNN-AE and avoid biased training.

One approach that one may think of to rectify the angles is to wrap the angles into  $[0,\,2\pi)$  using a simple function  $g(\phi)=\mathrm{mod}(\phi,2\pi)$ . This approach, however, is not effective. Fig. 9 shows an example of this rectification function. It can be seen that the rectified angle curve appears to be discontinuous. However, the discontinuity of the rectified data cannot be captured by the DNN-AE, as illustrated in the figure. Therefore, a continuous rectification function is needed for the preprocessing of  $\Phi$ .

In light of this requirement, we propose a piece-wise function to rectify the angles in  $\Phi$  before feeding them into the DNN-AE:

$$g(\phi_k) = \begin{cases} \frac{1}{2\pi} (\phi_k - 0.07) & \text{if } \min_k(\phi_k) < 0, \\ \frac{1}{2\pi} (\phi_k - 6.16) & \text{if } \max_k(\phi_k) > 2\pi, \\ \frac{1}{\pi} (\phi_k - 3.13) & \text{otherwise,} \end{cases}$$
 (2)

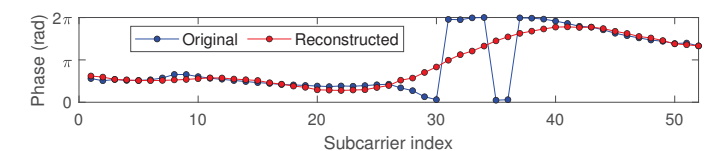


Fig. 9: Illustrating the underlying problem of the rectification function  $g(\phi) = \text{mod}(\phi, 2\pi)$  for the angles in  $\Phi$ .

for  $k=1,2,\cdots,52$ . In this equation, the values of 0.07,6.16, and 3.13 are the mean of the angles in their respective category and obtained from our experimental measurements.

Fig. 8(b) shows the PDF and subcarrier-wise variance of all the angles in  $\Phi$  after preprocessing. Compared to the distribution and variance before preprocessing as shown in Fig. 8(a), it is evident that this preprocessing can flatten both probability and variance distributions, making the DNN-AE easy to converge.

Given that  $g(\phi_k)$  is used for data preprocessing on the encoder side, an inverse function is needed on the decoder side to recover the original angles. However,  $g(\phi_k)$  is a piece-wise function and it is not invertible. To address this challenge, we use two bits to indicate the sub-function used for rectification, i.e., "00" means  $g(\phi_k) = \frac{1}{2\pi}(\phi_k - 0.07)$ , "01" means  $g(\phi_k) = \frac{1}{2\pi}(\phi_k - 6.16)$ , and "10" means  $g(\phi_k) = \frac{1}{\pi}(\phi_k - 3.13)$ . With these two bits, the decoder is capable of constructing  $g^{-1}(\phi_k)$  and inversing the preprocessing at the encoder. In the exploitation phase, each STA should send these indication bits to the AP via the over-the-air uplink channel. It is worth noting that these indication bits are of very small size compared to conventional CSI feedback.

#### D. Online Training: Settings and Procedure

**Training Procedure and Hyper-Parameter Tuning:** We train the DNN-AEs shown in Fig. 6 using the preprocessed datasets. For the two DNN-AEs, each hidden layer is composed of a fully-connected layer followed by a batch-normalization layer to speed up the training convergence [36]. Also, rectified linear unit (ReLU) activation function is used. The DNN-AEs are trained to minimize loss function, which is defined as:

$$L(\mathbf{x}, \hat{\mathbf{x}}) = \frac{\|\hat{\mathbf{x}} - \mathbf{x}\|}{\|\mathbf{x}\|},\tag{3}$$

where x and  $\hat{x}$  represent the input sample and the corresponding reconstructed sample, respectively. The networks are trained using Adam optimizer [37]. We started the training with an initial learning rate of 0.001 and reduced it with a decay rate of 0.98 following a step-wise approach. All parameters were initialized using Xavier initialization [38]. Dropout [39] is applied to hidden layers to prevent overfitting and improve the generalization of the model. The final architectures are the result of random search over hyperparameters. All DNN-AEs are trained end-to-end using Pytorch v1.4 library [40].

**Readiness of DNN-AEs for Exploitation:** While the AP trains the DNN-AEs whenever it receives a batch of CSI reports from the STAs, a question to ask is about the criteria for the completion of its training phase. In our experiments,

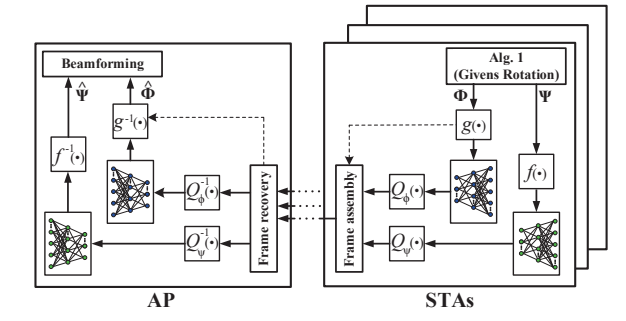


Fig. 10: CSI compression at STA and decompression at AP.

we check the loss function of validation data to determine the readiness of the DNN-AEs. If the loss function of validation data is consistently less than 1.5%, we consider the completion of the training phase and readiness of DNN-AEs. The AP then broadcasts the parameters of the encoder parts of the two DNN-AEs as well as the preprocessing parameters to the STAs, so that the STAs can reconstruct the encoder part to compress the angles in  $\Psi$  and  $\Phi$ , as shown in Fig. 1(b). Using 32 bits to represent each parameter (real number), the total overhead of transmitting the parameters of the trained DNN-AEs is 5.74 kB, where 1.80 kB is for the parameters of  $\Psi$ 's DNN-AE, and 3.94 kB is for the parameters of  $\Phi$ 's DNN-AE. This airtime overhead of DNN-AEs broadcast is not an issue for two reasons. First, the broadcast takes place once for a long time period. Second, the broadcast is not time-sensitive and the AP can broadcast whenever it gets the resource.

**Keep Training DNN-AEs:** While the AP has broadcast the DNN-AEs to the STAs, there might be some STAs incapable of utilizing the DNN-AEs for CSI compression. For example, some incumbent STAs may support MU-MIMO but do not support autoencoder-based CSI compression. In such a case, the AP can instruct these STAs to report CSI without compression and use the uncompressed CSI reports for the construction of beamforming filters as that in exiting 802.11 protocols. In the meantime, the AP can use the uncompressed CSI reports from those STAs to keep training the DNN-AEs.

**Updating DNN-AEs:** During the training in exploitation phase, the AP will periodically use validation data to check the loss function. It rebroadcasts the DNN-AEs to STAs whenever it detects a stable improvement in trained DNN-AEs. Furthermore, the AP rebroadcasts the updated DNN-AEs to the STAs whenever it observes an increase (e.g., 5%) in downlink packet error rate. Such an event simply means that the DNN-AEs in use are outdated. We note that we did not observe a failure of the DNN-AEs in our experiments even though we moved the testbed significantly. We employ this mechanism just to improve the robustness of our design.

#### E. Real-Time DNN-AEs Exploitation: CSI Compression

When the AP completes the training phase, the WLAN enters into the exploitation phase. In this phase, the AP and STAs still use the existing MU-MIMO protocols shown in Fig. 2 for downlink MU-MIMO transmissions, except that DNN-AEs are used for CSI compression of the channel

feedback. In what follows, we describe CSI compression at an STA and CSI decompression at the AP, respectively.

STA-Side Operations: Fig. 10 shows the CSI compression operations at a STA. The STA first estimates the CSI and then converts the estimated CSI to two sets of angles. Then, the two sets of angles are preprocessed and fed into the encoders of DNN-AEs for compression. After that, quantization is performed on the output, followed by frame assembly for uplink CSI report. A question to ask is how many bits should be used for quantization of the output of DNN-AEs' encoders. While there is no analytical guidance to answer this question, we resort to experimental tests. We found that the angles in  $\Phi$ are more sensitive to quantization errors than the angles in  $\Psi$ . We also observed that the setting of 5 bits for each output of  $\Psi$ 's DNN-AE and 8 bits for each output of  $\Phi$ 's DNN-AE is a good trade-off between performance and airtime overhead. In our experiments, we will stick to this quantization setting. AP-Side Operations: Fig. 10 shows the CSI decompression operations at the AP, which try to recover the original CSI based on the compressed angles. The decompressed CSI will be used to construct the beamforming filters (e.g., using SVDbased precoding methods) for downlink MU-MIMO.

#### F. Compression Ratio and Airtime Overhead

As presented in Section III-A, existing MU-MIMO protocols employ two options for CSI feedback quantization and can group different numbers of subcarriers for CSI feedback. The number of bits required for CSI feedback can be expressed as  $N_{\rm sc}N_{\rm a}(p+q)/N_{\rm g}$ , where  $N_{\rm sc}$  is the number of valid subcarriers,  $N_a$  is the number of angle sequences in  $\Psi$  or  $\Phi$ , p and q are the number of quantization bits as shown in Alg. 1, and  $N_{\rm g}$  is the number of subcarriers in a group. Per IEEE 802.11ac, we have  $(p,q) \in \{(5,7),(7,9)\}, N_{\rm g} \in \{1,2,4\}$ .

LB-SciFi uses two DNN-AEs to compress the angle sequences in  $\Psi$  or  $\Phi$ . Based on the DNN-AEs settings and quantization bits as shown in Fig. 10, the number of feedback bits is  $N_a(5\times 3+8\times 8+2)=81N_a$ . Therefore, the compression ratio of LB-SciFi can be written as:

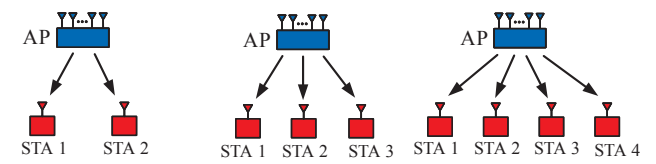
$$compression\_ratio = 1 - \frac{81N_g}{52(p+q)},$$
 (4)

where  $(p,q) \in \{(5,7),(7,9)\}$  and  $N_g \in \{1,2,4\}$  as per [1]. Based on (4), it is easy to check that LB-SciFi can achieve

significant compression compared to the existing protocols. The compression ratio ranges from 48.1% to 90.3%, depending on the setting of the existing channel feedback protocols. While LB-SciFi significantly reduces the quantity of CSI feedback, a question to ask is about the quality of its compressed feedback, including the feedback error and the impact on downlink MU-MIMO data rate. We will provide experimental results to answer this question in the next section.

#### G. Limitations

Some limitations of LB-SciFi are discussed as follows. **Compression Settings:** LB-SciFi involves many parameters such as number of layers in DNN-AEs, number of neurons on each layer, number of bits for quantization, and



(a) Two-user case. (b) Three-user case. (c) Four-user case.

Fig. 11: Experimental setup for downlink MU-MIMO.

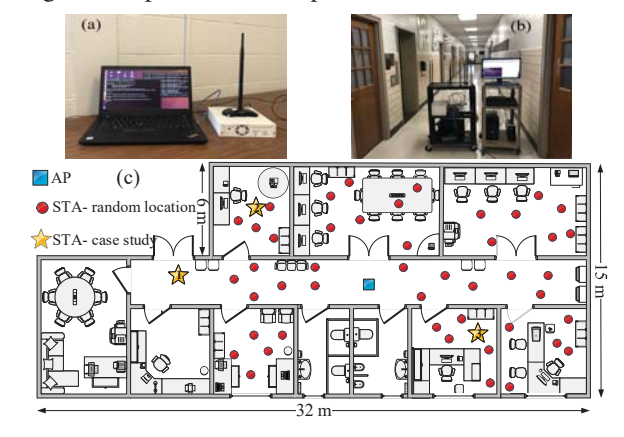


Fig. 12: Illustrating our wireless testbed and test environment. (a) Prototyped STA. (b) Prototyped AP. (c) Floor plan of tests.

the preprocessing functions parameters. These parameters are empirically chosen in our design, and there is no systematic approach to determine the optimal values of those parameters. Indeed, LB-SciFi is essentially heuristic and cannot offer any guarantee on its compression loss performance.

**Dataset Size:** The key phase of LB-SciFi is training the two DNN-AEs. However, there is no guideline on how many data samples suffice for the two DNN-AEs' training. Our experiments show that 13,100 data samples can achieve at least 98.5% compression accuracy. However, this number is not generic and may change in other network environments. In general, the size of required training dataset is unknown.

Variability of Physical Environment: When there is a significant change in the surroundings of the AP (e.g., a metal desk placed in front of the AP or the AP is moved into a distinct environment), re-training will be triggered to update the DNN-AEs. LB-SciFi cannot offer a time guarantee on the re-training as it depends on the speed of data collection.

# V. EXPERIMENTAL EVALUATION

In this section, we evaluate the performance LB-SciFi in comparison with existing 802.11 protocols in an indoor wireless environment. For ease of exposition, we use 802.11- TiGj (or simply TiGj) to denote the IEEE 802.11 MU-MIMO protocol with Type i feedback and j subcarriers in a group, where  $i \in \{0,1\}$  and  $j \in \{1,2,4\}$  (see Section III-A and [1]). Since T1G1 represents the finest feedback and T0G4 represents the coarsest feedback, we will use these two protocols as our performance comparison baseline.

#### A. Experimental Setup and Implementation

**Downlink MU-MIMO:** We consider a WLAN as shown in Fig. 11, where the AP can serve two, three, or four STAs

simultaneously. When the AP obtains the compressed CSI reports from the STAs, it first recovers the required spatial information and then constructs the beamforming filters. While there are many different precoding methods in the literature, we used zero-forcing precoding method in our experiments owing to its popularity and ease of implementation.

Implementation of AP and STAs: Fig. 12(a–b) shows our wireless testbed. The AP and STAs are built using USRP N210 devices and general-purpose computers. Each USRP N210 device is equipped with VERT2450 Antenna for radio signal transmission/reception at 2.484 GHz. The computers are used for baseband signal processing and MAC protocol implementation. More specifically, the AP is implemented using a Dell Inspiron 3671 Desktop, which serves eight USRP N210 devices through a 10Gb fiber optic cable and a DGS-1210-20/ME Ethernet switch. Each STA is prototyped with a Lenovo ThinkPad T480 and one USRP N210 device.

Implementation of 802.11 Protocols: IEEE 802.11 protocols are implemented with the legacy PHY and MAC layers specifications. We use IEEE 802.11 frame format with 64 subcarriers for OFDM modulation. Out of these 64 subcarriers, 48 subcarriers carry payload and 4 subcarriers contain pilots. The sampling rate and carrier frequency are set to 20 MSps and 2.484 GHz, respectively. Also, the maximum transmission power is set to 15 dBm. All the necessary 802.11 baseband signal processing modules are realized with C++ in GNU Radio. For ease of implementation, our 802.11 protocols do not include user scheduling.

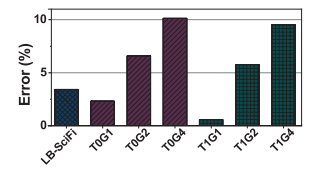
**Implementation of LB-SciFi:** LB-SciFi is implemented on top of 802.11 protocols. It mainly deals with collecting datasets and training DNN-AEs. On our testbed, the training datasets are automatically generated in the 802.11 protocols. With the collected datasets, DNN-AEs are trained end-to-end using Pytorch v1.4 library [40] and Adam optimizer [37].

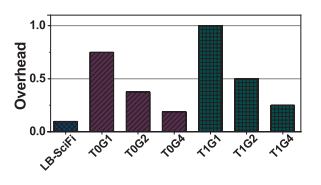
**Experimental setting:** Fig. 12(c) shows an office scenario where we conducted the experiments. The AP is placed at the spot marked as a blue square in the figure, while each STA is placed at a random location marked as a red circle.

#### B. DNN-AEs Training and Feedback

**Data Collection Campaign:** We ran the MU-MIMO communications shown in Fig. 11(c) to collect data for DNN-AEs training at the AP. The data collection campaign was conducted during two weekdays from 10am to 8pm. The human activity level in the environment was high between 11am to 2pm and low to moderate in other periods of time. To cover all areas, we were moving the STAs around all locations. This can be achieved in real systems thanks to the mobility of some Wi-Fi devices such as phones and laptops. In our experiments, the AP eventually collected 60,000 samples for training the DNN-AEs.

Sufficiency of Collected Data: We conduct convergence test under two criteria: i) the test loss of DNN-AE should be less than 1.5%, and ii) the loss difference for two validations should be less than 0.1%. With such two criteria,  $\Psi$ 's DNN-AE converges with 7,300 samples, and  $\Phi$ 's DNN-AE





(a) Normalized feedback error

(b) Normalized feedback overhead

Fig. 13: Feedback comparison between LB-SciFi and 802.11 protocols (T0G1, T0G2, T0G4, T1G1, T1G2, and T1G4).

TABLE I: EVM specification in IEEE 802.11ac standard [1].

EVM (dB)	(inf -5)	[-5 -10)	[-10 -13)	[-13 -16)	[-16 -19)	[-19 -22)	[-22 -25)	[-25 -27)	[-27 -30)	[-30 -32)	[-32 -inf)
Modulation	N/A	BPSK	QPSK	QPSK	16QAM	16QAM	64QAM	64QAM	64QAM	256QAM	256QAM
Coding rate	N/A	1/2	1/2	3/4	1/2	3/4	2/3	3/4	5/6	3/4	5/6
γ(EVM)	0	0.5	1	1.5	2	3	4	4.5	5	6	20/3

converges with 13,100 samples. This indicates that 60,000 samples suffice for training DNN-AEs.

Computational Complexity of Training: In our experiments, the training process takes less than 5 seconds on a Desktop PC with i5 CPU and 16 GB memory. A question is how much time is needed for training DNN-AEs on a commodity AP (Wi-Fi router). Since most commodity APs are equipped with an ARM processor, we expect that a commodity AP may take minutes to complete the training. In addition, we note that the training process is not time-sensitive, and an AP can take its spare time to complete the training. If an AP is not capable of doing the training by itself, it can take advantage of its wired Internet connection and a cloud server to run the training.

**Feedback Error:** With the completion of the first training, we examine the performance of the DNN-AEs. LB-SciFi introduces CSI error during the feedback. The feedback error can be attributed to two sources: *compression* and *quantization*. The compression error comes from the imperfection of the DNN-AEs, and the quantization error comes from the limited quantization bits. The normalized feedback error can be quantified by the loss function in (3). Fig. 13(a) shows our measured normalized feedback errors. It can be seen that LB-SciFi has a larger feedback error than 802.11-T0G1/T1G1 protocols, and it has a smaller feedback error compared to 802.11-T0G2/T0G4/T1G2/T1G4 protocols. This is because 802.11-T0G1/T1G1 protocols do not compress the CSI in the spectral domain while other protocols naively compress CSI in the spectral domain.

Feedback Overhead: While LB-SciFi introduces larger error than 802.11-T0G1 and 802.11-T1G1, it uses much smaller uplink airtime resource for CSI feedback and therefore entails much smaller overhead. Fig. 13(b) compares the normalized feedback overhead of LB-SciFi with the existing 802.11 protocols. It can be seen that LB-SciFi entails much less overhead compared to 802.11 protocols. LB-SciFi's overhead is 0.1 while the lowest normalized overhead among IEEE 802.11 protocols is 0.2. Also, LB-SciFi's compression ratio ranges from 48.1% to 90.3%, thereby conserving much airtime resource for data transmissions.

# C. LB-SciFi: Performance Metrics

We now focus on the overall performance of downlink MU-MIMO. We will consider the following performance metrics.

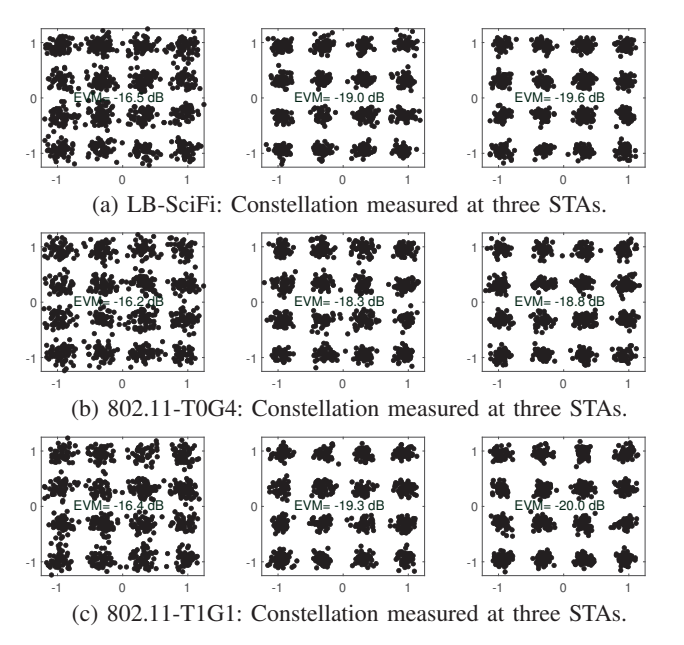


Fig. 14: Constellations of decoded signals at STAs when using LB-SciFi, 802.11-T0G4, and 802.11-T1G1.

Error Vector Magnitude (EVM): EVM is widely used to assess the quality of received signals at a receiver device. It is defined as follows:  $\text{EVM} = 10\log_{10}\left(\frac{\mathbb{E}[|\hat{X}-X|^2]}{\mathbb{E}[|X|^2]}\right)$ , where X and  $\hat{X}$  are the original and estimated signals, respectively.

**Gross Throughput:** Gross throughput refers to the data rate achieved by a device (AP or STA) without taking into account the CSI overhead. For STA i, based on the EVM of its decoded signal, its gross throughput can be extrapolated as follows:  $r_i = \frac{N_{\rm sp}}{N_{\rm fft} + N_{\rm cp}} \cdot b \cdot \gamma \, ({\rm EVM}_i)$ , where  $N_{\rm sp} = 48$  is the number of subcarriers carrying payload,  $N_{\rm fft} = 64$  is FFT points,  $N_{\rm cp} = 16$  is the length of cyclic prefix,  $b = 20 \times 10^6$  is the sampling rate,  ${\rm EVM}_i$  is EVM of the STA i's decoded signal, and  $\gamma({\rm EVM}_i)$  is the average number of bits carried by one subcarrier. This parameter is given in Table I. As such, the gross throughput at the AP can be computed by  $r = \sum_i r_i$ . **Net Throughput:** The net throughput refers to the data rate

subcarrier. This parameter is given in Table I. As such, the gross throughput at the AP can be computed by  $r = \sum_i r_i$ . **Net Throughput:** The net throughput refers to the data rate achieved by a device after subtracting the overhead mainly caused by CSI feedback in the MU-MIMO protocols. Denote  $\bar{r}$  as the net throughput achieved by the AP. Then, it can be expressed by:  $\bar{r} = \frac{\sum_i t_i r_i}{\max_i \{t_i\} + t_{\text{overhead}}}$ , where  $t_{\text{overhead}}$  is the time duration of overhead (NDPA, NDP, Poll, CBR, and ACK) and  $t_i$  is the time duration required by STA i for its downlink data transmission (see Fig. 2). While the value of  $t_{\text{overhead}}$  is fixed, the value of  $t_i$  is not.  $t_i$  is determined by the downlink data packet size and selected modulation and coding scheme. In real WLANs, a data packet should not exceed 2304 bytes [41]. In our experiments, we consider the maximum packet size to measure the lowest throughput gain that can be achieved by LB-SciFi.

### D. Micro Performance of LB-SciFi: A Case Study

We use a case study to examine the micro performance of LB-SciFi. We consider the network shown in Fig 11(b) and

TABLE II: Experimental results of the case study for comparing LB-SciFi with 802.11 protocols.

		STA 1	STA 2	STA 3	AP
LB-SciFi	EVM (dB)	-16.5	-19.0	-19.6	-
	Feedback overhead (kbit)	0.6	0.6	0.6	-
	Gross throughput (Mbps)	24.0	36.0	36.0	96.0
	Net throughput (Mbps)	15.9	23.9	23.9	63.7
T0G4	EVM (dB)	-16.2	-18.3	-18.8	_
	Feedback overhead (kbit)	1.1	1.1	1.1	-
	Gross throughput (Mbps)	24.0	24.0	24.0	72.0
	Net throughput (Mbps)	15.0	15.0	15.0	45.0
T1G1	EVM (dB)	-16.4	-19.3	-20.0	_
	Feedback overhead (kbit)	5.8	5.8	5.8	-
	Gross throughput (Mbps)	24.0	36.0	36.0	96.0
	Net throughput (Mbps)	9.4	14.1	14.1	37.6

place the three STAs at the spots marked with golden stars in Fig. 12(c). We compare the performance of LB-SciFi with 802.11-T1G1/T0G4 protocols.

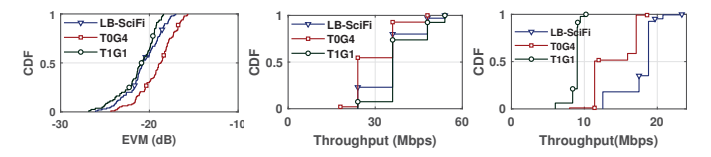
EVM: We conduct downlink MU-MIMO transmissions using LB-SciFi, 802.11-T0G4, and 802.11-T1G1. Fig. 14 exhibits the constellation of the decoded data packet at each STA with the three protocols. As shown in Fig. 14(a), LB-SciFi achieved –16.5 dB EVM at STA 1, –19.0 dB EVM at STA 2, and –19.6 dB EVM at STA 3. In contrast, Fig. 14(b) shows the achieved EVM at the three STAs when 802.11-T0G4 is used; and Fig. 14(c) shows the achieved EVM at the three STAs when 802.11-T1G1 is used. It can be seen that LB-SciFi achieves an EVM performance similar to 802.11-T1G1 and outperforms 802.11-T0G4. We note that the constellations in Fig. 14 can be successfully decoded thanks to the powerful LDPC channel code. It is also worth pointing out that LB-SciFi can support any modulation and coding scheme as long as channel quality permits.

**Feedback Overhead:** In the MU-MIMO transmissions, the CSI reports are transmitted from STAs to the AP using BPSK rate to ensure the feedback reliability [18]. Table II lists the feedback overhead using different protocols. As we can see from the table, LB-SciFi entails 0.6 kbit feedback overhead per STA. In contrast, 802.11-T0G4 entails 1.1 kbit feedback overhead per STA, and 802.11-T1G1 entails 5.8 kbit feedback overhead per STA.

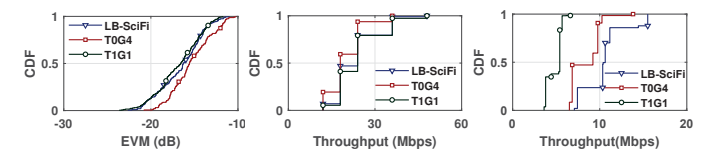
**Gross and Net Throughput:** Table II lists each STA's and the AP's gross/net throughput. We can see that LB-SciFi's gross throughput is larger than 802.11-T0G4 but less than 802.11-T1G1. However, LB-SciFi's net throughput is larger than both of them. The overall net throughput gain of LB-SciFi is 41.7% over 802.11-T0G4 and 68.8% over 802.11-T1G1.

# E. Macro Performance of LB-SciFi: Extensive Results

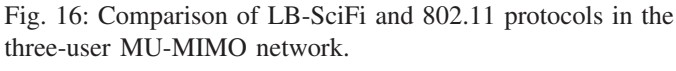
We now extend our case study to a more generic scenario. We consider the three networks in Fig. 11 and measure their performance at many different locations as shown in Fig. 12. Our evaluation methodology follows the previous case study. **Two-User MIMO:** Fig. 15 presents the cumulative distribution function (CDF) of our measured EVM, gross throughput, and net throughput over all locations when the AP serves two STAs. Per Fig. 15(a), the average EVM of decoded signals at the two STAs is -20.7 dB for LB-SciFi, -19.1 dB for 802.11-T0G4, and -21.2 dB for 802.11-T1G1. Compared to 802.11-



(a) EVM (b) Gross throughput (c) Net throughput Fig. 15: Comparison of LB-SciFi and 802.11 protocols in the two-user MU-MIMO network.



(a) EVM (b) Gross throughput (c) Net throughput Fig. 16: Comparison of LB-SciFi and 802.11 protocols in the



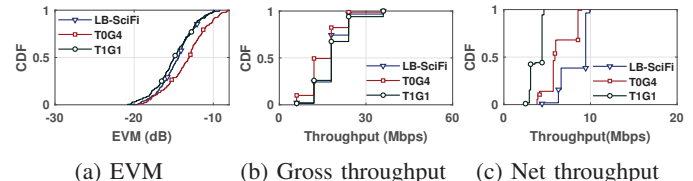


Fig. 17: Comparison of LB-SciFi and 802.11 protocols in the four-user MU-MIMO network.

T0G4, LB-SciF has 1.6 dB EVM improvement. Compared to 802.11-T1G1, LB-SciF has 0.5 dB EVM degradation. Per Fig 15(b), LB-SciFi achieves an average of 35.8 Mbps per-STA gross throughput, while 802.11-T0G4 and 802.11-T1G1 achieve 30.2 Mbps and 38.7 Mbps, respectively. Per Fig 15(c), LB-SciFi achieves an average of 17.6 Mbps per-STA net throughput, while 802.11-T0G4 and 802.11-T1G1 achieve 14.1 Mbps and 8.8 Mbps, respectively. The results indicate that LB-SciFi offers 25.0% net throughput gain over 802.11-T0G4 and 99.8% gain over 802.11-T1G1.

[31] proposed a 3-dimensional (time, frequency, and quantization) adaptive feedback compression (AFC) scheme for WLANs. While LB-SciFi is orthogonal to the time-domain AFC, we compare LB-SciFi with the frequency-domain AFC. Experimental results in [31] show the frequency-domain AFC achieves 12.7% throughput gain when compared to 802.11-T1G1. LB-SciFi achieves an average of 99.8% throughput gain over 802.11-T1G1. The comparison result is not surprising, as LB-SciFi exploits DNN-AEs to reduce channel's intersubcarrier correlation for feedback compression, rather than grouping a subset of subcarriers for feedback compression.

Three-User MIMO: Fig. 16 presents the CDF of our measured EVM, gross throughput, and net throughput over all locations when the AP serves three STAs. Per Fig 16(a), the average EVM of decoded signals at the three STAs is -16.5 dB for LB-SciFi, -15.3 dB for 802.11-T0G4, and -16.8 dB for 802.11-T1G1. Per Fig 16(b), LB-SciFi achieves an average of 23.3 Mbps per-STA gross throughput, while 802.11-T0G4 and 802.11-T1G1 achieve 20.0 Mbps and 24.0 Mbps, respectively. Per Fig 16(c), LB-SciFi achieves an

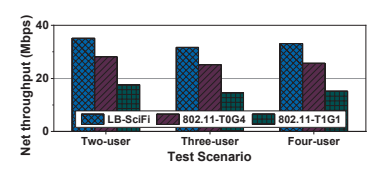


Fig. 18: Net throughput of LB-SciFi and 802.11 protocols.

average of 10.5 Mbps per-STA net throughput, while 802.11-T0G4 and 802.11-T1G1 achieve 8.4 Mbps and 4.9 Mbps, respectively. Therefore, LB-SciFi offers 25.7% net throughput gain over 802.11-T0G4 and 116.8% net throughput gain over 802.11-T1G1.

**Four-User MIMO:** Fig. 17 presents the CDF of our measured EVM, gross throughput, and net throughput over all the locations when the AP serves two STAs. Per Fig 17(a), the average EVM of decoded signals at the four STAs is -14.5 dB for LB-SciFi, -13.4 dB for 802.11-T0G4, and -14.9 dB for 802.11-T1G1. Per Fig 17(b), LB-SciFi achieves an average of 18.3 Mbps per-STA gross throughput, while 802.11-T0G4 and 802.11-T1G1 achieve 15.6 Mbps and 19.0 Mbps, respectively. Per Fig 17(c), LB-SciFi achieves an average of 8.3 Mbps per-STA net throughput, while 802.11-T0G4 and 802.11-T1G1 achieve 6.4 Mbps and 3.8 Mbps, respectively. Therefore, LB-SciFi offers 28.9% net throughput gain over 802.11-T0G4 and 117.3% net throughput gain over 802.11-T1G1.

Summary of Observations We now focus on the net throughput achieved by the AP. Fig. 18 depicts the total net throughput achieved by the AP when it employs these three protocols. As it can be seen, the three protocols yield similar throughput in two-user, three-user, and four-user MIMO cases. On average, LB-SciFi achieves 26.5% net throughput gain compared to 802.11-T0G4 and 111.3% throughput gain over 802.11-T1G1.

#### VI. CONCLUSION

In this paper, we presented LB-SciFi, an online learningbased channel feedback framework for existing IEEE 802.11 MU-MIMO protocols. LB-SciFi reduces the CSI feedback overhead for 802.11 protocols by leveraging recent advances in deep neural networks to compress CSI in the spectral domain without compromising the CSI feedback accuracy. The key component of LB-SciFi is an online training scheme, which requires no dedicated training datasets but takes advantage of available side information from existing 802.11 protocols to train the autoencoders. As such, LB-SciFi can be easily plugged into existing 802.11 protocols and thus amenable to practical implementation. We have built a prototype of LB-SciFi on a wireless testbed and evaluated its performance in indoor wireless environments. Experimental results show that LB-SciFi can reduce the feedback overhead by 73% and increases the network throughput by 69% on average.

#### ACKNOWLEDGMENT

We would like to thank our shepherd and anonymous reviewers for their valuable comments and feedback. This work was supported in part by NSF Grants CNS-1717840 and CNS-1846105. Part of this work was completed when the authors were with the University of Louisville.

#### REFERENCES

- [1] IEEE 802.11ac, "IEEE standard for information technology local and metropolitan area networks part 11: Wireless LAN medium access control (MAC) and physical layer (PHY) specifications amendment 5: Enhancements for higher throughput," IEEE Std. 802.11ac, 2014.
- [2] IEEE P802.11ax, "IEEE draft standard for information technology telecommunications and information exchange between systems local and metropolitan area networks specific requirements part 11: Wireless LAN medium access control (MAC) and physical layer (PHY) specifications amendment enhancements for high efficiency WLAN," IEEE P802.11ax/D4.0, pp. 1–746, March 2019.
- [3] K. Nishimori, T. Hiraguri, T. Mitsui, and H. Yamada, "Effectiveness of implicit beamforming with large number of antennas using calibration technique in multi-user MIMO system," *Electron.*, vol. 6, no. 4, p. 91, 2017.
- [4] X. Jiang, A. Decurninge, K. Gopala, F. Kaltenberger, M. Guillaud, D. Slock, and L. Deneire, "A framework for over-the-air reciprocity calibration for TDD massive MIMO systems," *IEEE Trans. Wireless Commun.*, vol. 17, no. 9, pp. 5975–5990, 2018.
- [5] X. Jiang and F. Kaltenberger, "Channel reciprocity calibration in TDD hybrid beamforming massive MIMO systems," *IEEE J. Sel. Topics Signal Process.*, vol. 12, no. 3, pp. 422–431, 2018.
- [6] H. Zhao, G. Pottie, and B. Daneshrad, "Reciprocity calibration of TDD MIMO channel for interference alignment," *IEEE Trans. Wireless Commun.*, 2020.
- [7] G. Redieteab, L. Cariou, P. Christin, and J.-F. Helard, "PHY+ MAC channel sounding interval analysis for IEEE 802.11 ac MU-MIMO," in *Proc. Int. Symp. Wireless Commun. Syst. (ISWCS)*, pp. 1054–1058, 2012.
- [8] E. Perahia and M. X. Gong, "Gigabit wireless LANs: An overview of IEEE 802.11 ac and 802.11 ad," ACM SIGMOBILE Mob. Comput. Commun. Rev., vol. 15, no. 3, pp. 23–33, 2011.
- [9] M. Yazid and A. Ksentini, "Modeling and performance analysis of the main MAC and PHY features of the 802.11 ac standard: A-MPDU aggregation vs spatial multiplexing," *IEEE Trans. Veh. Technol.*, vol. 67, no. 11, pp. 10243–10257, 2018.
- [10] J. Oh, H.-J. Hong, and H.-D. Choi, "Performance analysis for channel sounding in IEEE 802.11 ac network," in *Proc. Int. Conf. Inf. Commun. Technol. Convergence*, pp. 1240–1242, 2015.
- [11] T. Nabetani, N. Madhavan, H. Mori, and T. Aoki, "A novel low-overhead channel sounding protocol for downlink multi-user MIMO in IEEE 802.11 ax WLAN," *IEICE Trans. Commun.*, vol. 101, no. 3, pp. 924– 932, 2018.
- [12] O. Bejarano, E. Magistretti, O. Gurewitz, and E. W. Knightly, "MUTE: Sounding inhibition for MU-MIMO WLANs," in *Proc. 11th Annu. IEEE Int. Conf. Sens.*, Commun., Netw. (SECON), pp. 135–143, 2014.
- [13] X. Ma, Q. Gao, J. Wang, V. Marojevic, and J. H. Reed, "Dynamic sounding for multi-user MIMO in wireless LANs," *IEEE Trans. Consum. Electron.*, vol. 63, no. 2, pp. 135–144, 2017.
- [14] T. Kuber, D. Saha, and I. Seskar, "Predicting channel transition for MU-MIMO beamforming," in *Proc. IEEE 5G World Forum (5GWF)*, pp. 83–88, 2018.
- [15] J. Choi, S. Choi, and K. B. Lee, "Sounding node set and sounding interval determination for IEEE 802.11 ac MU-MIMO," *IEEE Trans.* Veh. Technol., vol. 65, no. 12, pp. 10069–10074, 2016.
- [16] R. E. Guerra, N. Anand, C. Shepard, and E. W. Knightly, "Opportunistic channel estimation for implicit 802.11 af MU-MIMO," in *Proc. 28th Int. Teletraffic Congr. (ITC)*, vol. 1, pp. 60–68, 2016.
- [17] H. Zeng, "INFB: A low-overhead downlink MU-MIMO scheme for wireless LANs," in *Proc. IEEE Int. Conf. Netw. Protocols (ICNP)*, pp. 389–399, 2018.
- [18] H. Lou, M. Ghosh, P. Xia, and R. Olesen, "A comparison of implicit and explicit channel feedback methods for MU-MIMO WLAN systems," in *Proc. IEEE 24th Annu. Int. Symp. Personal Indoor Mobile Radio Commun. (PIMRC)*, pp. 419–424, 2013.
- [19] X. Li and H. Wu, "Spatio-temporal representation with deep neural recurrent network in MIMO CSI feedback," *IEEE Wireless Commun. Lett.*, 2020.
- [20] T. Wang, C.-K. Wen, S. Jin, and G. Y. Li, "Deep learning-based CSI feedback approach for time-varying massive MIMO channels," *IEEE Wireless Commun. Lett.*, vol. 8, no. 2, pp. 416–419, 2018.

- [21] C. Lu, W. Xu, H. Shen, J. Zhu, and K. Wang, "MIMO channel information feedback using deep recurrent network," *IEEE Commun. Lett.*, vol. 23, no. 1, pp. 188–191, 2019.
- [22] C.-K. Wen, W.-T. Shih, and S. Jin, "Deep learning for massive MIMO CSI feedback," *IEEE Wireless Commun. Lett.*, vol. 7, no. 5, pp. 748–751, 2018.
- [23] J. Guo, C.-K. Wen, S. Jin, and G. Y. Li, "Convolutional neural network based multiple-rate compressive sensing for massive MIMO CSI feedback: Design, simulation, and analysis," *IEEE Trans. Wireless Commun.*, 2020.
- [24] Q. Yang, M. B. Mashhadi, and D. Gündüz, "Deep convolutional compression for massive MIMO CSI feedback," in *Proc. IEEE Int. Workshop Mach. Learn. Signal Process. (MLSP)*, pp. 1–6, 2019.
  [25] Y. Liao, H. Yao, Y. Hua, and C. Li, "CSI feedback based on deep
- [25] Y. Liao, H. Yao, Y. Hua, and C. Li, "CSI feedback based on deep learning for massive MIMO systems," *IEEE Access*, vol. 7, pp. 86810– 86820, 2019.
- [26] Y. Yang, F. Gao, G. Y. Li, and M. Jian, "Deep learning-based downlink channel prediction for FDD massive MIMO system," *IEEE Commun. Lett.*, vol. 23, no. 11, pp. 1994–1998, 2019.
- [27] Z. Liu, L. Zhang, and Z. Ding, "Exploiting bi-directional channel reciprocity in deep learning for low rate massive MIMO CSI feedback," *IEEE Wireless Commun. Lett.*, vol. 8, no. 3, pp. 889–892, 2019.
- [28] M. S. Safari, V. Pourahmadi, and S. Sodagari, "Deep UL2DL: Data-driven channel knowledge transfer from uplink to downlink," *IEEE Open J. Veh. Technol.*, vol. 1, pp. 29–44, 2019.
- [29] Y. Jang, G. Kong, M. Jung, S. Choi, and I.-M. Kim, "Deep autoencoder based CSI feedback with feedback errors and feedback delay in FDD massive MIMO systems," *IEEE Wireless Commun. Lett.*, vol. 8, no. 3, pp. 833–836, 2019.
- [30] J. H. Suh, J. Zhu, and O. Aboul-Magd, "System and method for quantization of angles for beamforming feedback," Feb. 6 2018. US Patent 9,887,749.
- [31] X. Xie, X. Zhang, and K. Sundaresan, "Adaptive feedback compression for mimo networks," in *Proc. ACM MobiCom*, pp. 477–488, 2013.
- [32] A. Humeau-Heurtier, C.-W. Wu, S.-D. Wu, G. Mahé, and P. Abraham, "Refined multiscale Hilbert–Huang spectral entropy and its application to central and peripheral cardiovascular data," *IEEE Trans. Biomed. Eng.*, vol. 63, no. 11, pp. 2405–2415, 2016.
- [33] D. Kim, "Normalization methods for input and output vectors in backpropagation neural networks," *Int. J. Comput. Math.*, vol. 71, no. 2, pp. 161–171, 1999.
- [34] Y. Le Cun, I. Kanter, and S. A. Solla, "Eigenvalues of covariance matrices: Application to neural-network learning," *Phys. Rev. Lett.*, vol. 66, no. 18, p. 2396, 1991.
- [35] Y. A. LeCun, L. Bottou, G. B. Orr, and K.-R. Müller, "Efficient backprop," in *Neural networks: Tricks of the trade*, pp. 9–48, Springer, 2012.
- [36] S. Ioffe and C. Szegedy, "Batch normalization: Accelerating deep network training by reducing internal covariate shift," arXiv preprint arXiv:1502.03167, 2015.
- [37] D. P. Kingma and J. L. Ba, "Adam: A method for stochastic optimization," Int. Conf. Learn. Represent., 12 2015.
- [38] X. Glorot and Y. Bengio, "Understanding the difficulty of training deep feedforward neural networks," in *Proc. Int. Conf. Artif. Intell. Stat.*, pp. 249–256, 2010.
- [39] N. Srivastava, G. Hinton, A. Krizhevsky, I. Sutskever, and R. Salakhutdinov, "Dropout: A simple way to prevent neural networks from overfitting," J. Mach. Learn. Res., vol. 15, no. 1, pp. 1929–1958, 2014.
- [40] A. Paszke, S. Gross, F. Massa, A. Lerer, J. Bradbury, G. Chanan, T. Killeen, Z. Lin, N. Gimelshein, L. Antiga, A. Desmaison, A. Kopf, E. Yang, Z. DeVito, M. Raison, A. Tejani, S. Chilamkurthy, B. Steiner, L. Fang, J. Bai, and S. Chintala, "Pytorch: An imperative style, high-performance deep learning library," in *Advances in Neural Information Processing Systems 32* (H. Wallach, H. Larochelle, A. Beygelzimer, F. d Alché-Buc, E. Fox, and R. Garnett, eds.), pp. 8024–8035, Curran Associates, Inc., 2019.
- [41] A. Perez, Wi-Fi Integration to the 4G Mobile Network. John Wiley & Sons Inc., 2018.